Laser-Induced Hydrothermal Growth of Heterogeneous Metal-Oxide Nanowire on Flexible Substrate by Laser Absorption Layer Design

Junyeob Yeo,[†,⊥] Sukjoon Hong,[‡,⊥] Gunho Kim,[§] Habeom Lee,[‡] Young Duk Suh,[‡] Inkyu Park,[§] Costas P. Grigoropoulos,[†] and Seung Hwan Ko[*,‡]

[†]Laser Thermal Lab, Department of Mechanical Engineering, University of California, Berkeley, California 94720, United States, [‡]Applied Nano and Thermal Science Lab, Department of Mechanical Engineering, Seoul National University, 1 Gwanak-ro, Gwanak-gu, Seoul 151-742, Korea, and [§]Department of Mechanical Engineering, Korea Advanced Institute of Science and Technology (KAIST), 291 Daehak-ro, Yuseong-gu, Daejeon 305-701, Korea. [⊥]Junyeob Yeo and Sukjoon Hong equally contributed to this work.

ABSTRACT Recent development of laser-induced hydrothermal growth enabled direct digital growth of ZnO nanowire array at an arbitrary position even on 3D structures by creating a localized temperature field through a photothermal reaction in liquid environment. However, its spatial size was generally limited by the size of the focused laser spot and the thermal diffusion, and the target material has been limited to ZnO. In this paper, we demonstrated a next generation laser-induced hydrothermal growth method to grow nanowire on a selected area that is even smaller than the laser focus size by designing laser absorption layer. The control of laser-induced temperature field was achieved through adjusting the physical properties of the substrate (dimension and thermal conductivity), and it enabled a successful synthesis of smaller nanowire array without changing any complex optics. Through precise localized temperature control with laser, this approach could be extended to various nanowires including ZnO and TiO_2 nanowires even on heat sensitive polymer substrate.

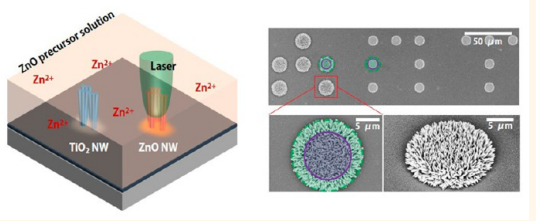

KEYWORDS: selective local laser growth · one-step direct growth · low temperature synthesis · hydrothermal growth · flexible substrate

Because of inherent difficulties in various manipulations and patterning techniques of nanomaterials such as Langmuir–Blogett,[1] dielectrophoresis,[2] self-assemble,[3] optical tweezer,[4] laser assisted pattering,[5] inkjet printing,[6,7] microcontact printing,[8] and microfluidics,[9] digital local synthesis of functional nanowire (NW) in liquid environment at high spatial precision has been one of the substantive issues for the facile fabrication of NW based microelectronic devices with ultrasmall size. Recently, local synthesis of NW array has been successfully achieved by localized micro/nano heating,[10,11] which is an easily accessible method that has wide applications in optoelectronics,[12] biology[13,14] and chemistry.[15] A most common scheme for micro/nano scale heating is an electrically driven Joule heater composed of a photolithographically patterned electrode layer operating under a constant bias voltage.[16,17] Its operation principle is very simple, however not applicable for the local synthesis of NWs at an arbitrary position since the local heating needs complex fabrication of microheater pattern connected to proper electrical power source and almost impossible for 3D complex system. Also, the implementation of the electrical Joule heating method in the liquid environment has the possibility of causing extra problems such as leakage current through the ionic precursor solution and a failure at the electrical contacts.

Recently, as an alternative to joule heating, Yeo *et al.* first introduced laser-induced local heating method as a novel scheme for digital local synthesis of NWs to broaden the applicability of the process to a great extent even on 3D structures[18] without the hassle of fabricating micro heater patterns. Through localized photothermal reaction, a

* Address correspondence to maxko@snu.ac.kr.

Received for review February 18, 2015 and accepted June 1, 2015.

Published online June 02, 2015
10.1021/acsnano.5b01125

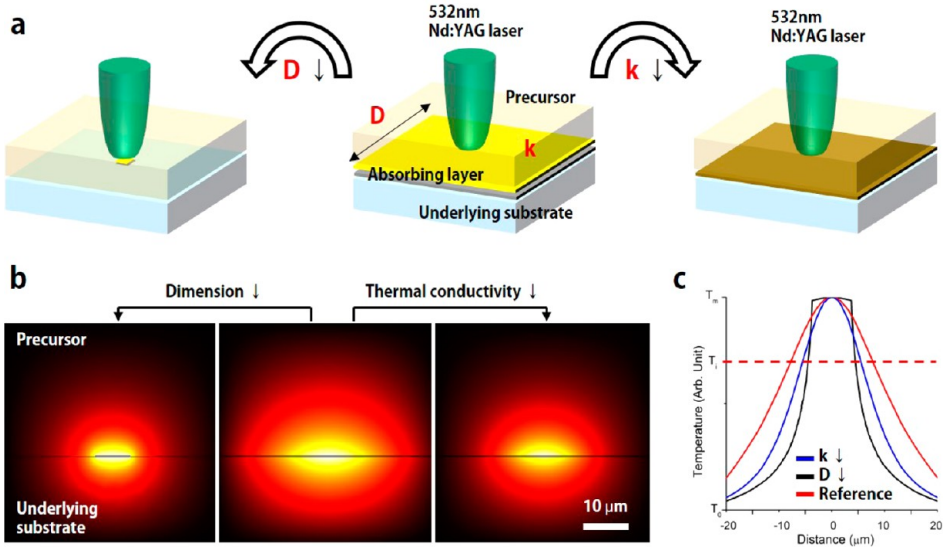

Figure 1. (a) Schematic illustration of the conventional LIHG (central picture) and proposed LIHG process (left and right picture). Either the physical size of the absorbing layer (*D*) or its thermal conductivity (*k*) can be altered to modify the profile of the laser-induced temperature field. (b) COMSOL simulation on the normalized temperature field profile according to either change in the laser absorbing layer. (c) Temperature profile at the solid−liquid interface. It is apparent that the resultant size subject to the initial growth (>T_i) shrinks for $D\downarrow$ or $k\downarrow$.

temperature field can be directly generated on the target substrate by laser-induced hydrothermal growth (LIHG), and its position is simply adjusted by changing the location of the focused laser spot.[19−22] Besides, although confined NWs array is easily obtained by LIHG process, its minimum nanowire growth array size was limited to >15 μm due to the diffraction limit of laser focusing spot, and the target material was demonstrated only for ZnO. The photothermal reaction and the resultant spatial heat diffusion of laser-induced temperature field are largely related to the size of focused spot at the target substrate, but it is often hard to change the focusing optics.[23−25] Such tight focusing also reduces the depth-of-focus and lowers the reproducibility of the process.[26]

Therefore, instead of reducing the focused laser spot, we investigated the influence of the laser absorption layer design on the laser-induced temperature field and subsequent local growth characteristics of NWs array. It is confirmed both in simulation and experiment that either the contraction in the physical size of the laser absorbing layer or the decrease in its thermal conductivity effectively shrinks the resultant temperature field induced by the focused laser without changing any optics. As a result, ZnO NW array at a diameter smaller than the focused laser spot has been obtained on the controlled target substrate. Moreover, through these studies on target substrate, we found that various NWs besides ZnO NW can be grown on specific flexible substrates, for the first time showing that LIHG process is compatible to other hydrothermally grown NWs as well. By applying two consecutive LIHG processes with different precursor solutions, ZnO NW and TiO_2 NW are simultaneously and selectively synthesized on the same substrate, which has potential applications in more sophisticated electronic devices such as multiplex environmental sensors.

Figure 1a shows the schematic illustration of the proposed LIHG process by laser absorption layer design. A visible laser beam is focused on the target substrate that consists of a laser absorbing layer, which is generally a thin metal layer at hundreds of nanometers, and an underlying substrate such as a glass wafer at macro-scale. The entire substrate is immersed in a transparent precursor solution that contains precursor ions and capping agents for further growth of the target nanostructure. The temperature increase is primarily confined at the laser focus and spread radially from the absorbing layer, while the exact profile should be determined by various heat transfer mechanisms including conduction through underlying substrate, thermal diffusion toward the absorbing layer and convection in the surrounding precursor solution.

The size of the resultant temperature field can be effectively reduced by either shrinking the physical dimension (*D*) of the absorption layer or decreasing its thermal conductivity (*k*). Since the absorption of visible wavelength in the underlying transparent substrate is practically negligible, the former spatially limits the area that is subject to the photothermal reaction, while the latter yields higher temperature gradient to constrict the overall size of the elevated temperature field. The temperature profile induced by a focused laser for either change is estimated prior to the experiment by conjugate heat transfer simulation. Every simulation has been conducted using COMSOL Multiphysics, whereas the photothermal reaction has been modeled as a surface heat flux at Gaussian shape according to

the intensity distribution of the laser beam with TEM_{00} mode. Its profile is assumed to be identical over time by neglecting the effect of the grown ZnO NW array. More detailed simulation parameters and chemical reaction behind LIHG process can be found in Supporting Information (Figure S1 and S2). The cross-sectional temperature profiles at the center of the focused laser spot are shown in Figure 1b, which qualitatively illustrate that the laser-induced temperature can be altered by changing the size or the thermal conductivity of the absorbing layer. For more comprehensive comparison, the normalized temperature profiles immediately above the absorbing layer are simultaneously drawn in Figure 1c. Although the laser parameters have remained unchanged in every case, the normalized temperature profiles are in discord with each other. Assuming that there exists maximum processing temperature (T_m) and the initial temperature (T_i) for effective growth of the target nanostructure, the spatial size subject to the NW growth should be suppressed in either case as shown in Figure 1c, although the actual temperature profile generally keeps changing as the laser-induced hydrothermal growth proceeds.

RESULTS AND DISCUSSION

As anticipated from the simulation, conventional LIHG process (Figure 1a, center picture) conducted on a target substrate with a metal thin film absorbing layer generally result in NW array larger than the focused laser spot due to high thermal conductivity of the metal layer. Figure 2a shows scanning electron microscopy (SEM) images of ZnO NW array grown on glass substrate with planar Au/Ti (thickness 220 nm/30 nm) absorbing layer according to different laser irradiation time at the laser power of 120 mW (see Figure S3 for detailed information on a single ZnO NW grown by LIHG process). The length distribution of ZnO NW array on a 2D plane after a complete growth resembles the temperature profile induced by a focused laser spot. The beam waist of the focused laser ($1/e^2$) has been estimated to be ~15 μm (denoted as green dot circle in Figure 2a) throughout the experiment, but the size of ZnO NW array subject to the initial growth exceeds the laser spot size and becomes even greater with the growth time as shown in Figure 2c, since the NW growth at the edge of the focused laser spot is slowly triggered at oblique angle due to the relatively low temperature compared to the center.[18]

The grown NW array size is effectively suppressed by limiting the size of laser absorbing layer by patterned metal layer. The thin metal patterns at circular shape with different diameters from 4 to 20 μm are created by conventional photolithography metal pattering process in order to investigate the effect of the laser absorption layer size on the grown NW array (see Figure S4 for detailed information on sample preparation for metal patterned on the glass substrate). As representative examples, the metal patterns at two different diameters, 4 and 10 μm, after the selective application of LIHG process are shown in Figure 2b while the laser power and the irradiation time have been maintained at 120 mW and 5 min in every case (see Figure S5 for LIHG applied on the metal patterns at different diameters). Because of the negligible photothermal reaction elsewhere, laser-induced temperature field is confined only in the vicinity of the circular metal pattern upon the laser irradiation. The resultant grown NW array sizes according to the metal pattern diameter are plotted in Figure 2d, showing that the NW array size smaller than the laser spot size can be achieved by reducing the laser absorption layer size. It is also noticeable that the ZnO NW grown on the confined metal patterns are more likely to be at an equal height since the temperature increase is uniform throughout the metal pattern as predicted from the simulation. While on the other hand, the digital nature of LIHG process is still valid, as confirmed in the Figure S6. It is expected that this scheme is further applicable to even smaller laser absorption layer patterns that are below the optical diffraction limit such as chemically synthesized nanomaterials. This approach hence will be very important for future nanosensor integration, which requires highly selective growth of functional nanomaterials on other nanostructures.

Another scheme proposed for the reduction of the array size is to use an absorbing layer with a low thermal conductivity. The thermal conductivity is basically determined by the material, however, in the case of thin light absorbing layer, the thermal conductivity can be effectively altered by changing the thickness of the metal film.[27−29] This idea has been further supported by the simulation in Figure S1. For the experiment, Au thin films at three different thicknesses, 30, 120, and 275 nm, are first deposited on the glass wafers with thermal evaporation. Subsequently, ZnO NW arrays are grown on these samples with fixed growth time (15 min), but at different laser powers, 50, 80, and 180 mW, which are ~90% of their threshold power for bubble nucleation. Assuming that the bubble always occurs at the same temperature, we estimate that the maximum temperatures are almost the same in every case, so that the effect of normalized temperature profile can be investigated. The optical microscopic images captured at the same magnification after the growth are shown in Figure 3a, showing that the ZnO NW array grown on a thicker metallic film shows bigger diameter. As these results are plotted in the graph as Figure 3b, it clearly shows that the resultant ZnO array size is controllable through alteration of the absorbing layer thickness. This result, together with the simulation result in Figure S1c, suggests that the size of ZnO NW array synthesized by LIHG can be very small on a bulk substrate that has low thermal conductivity such

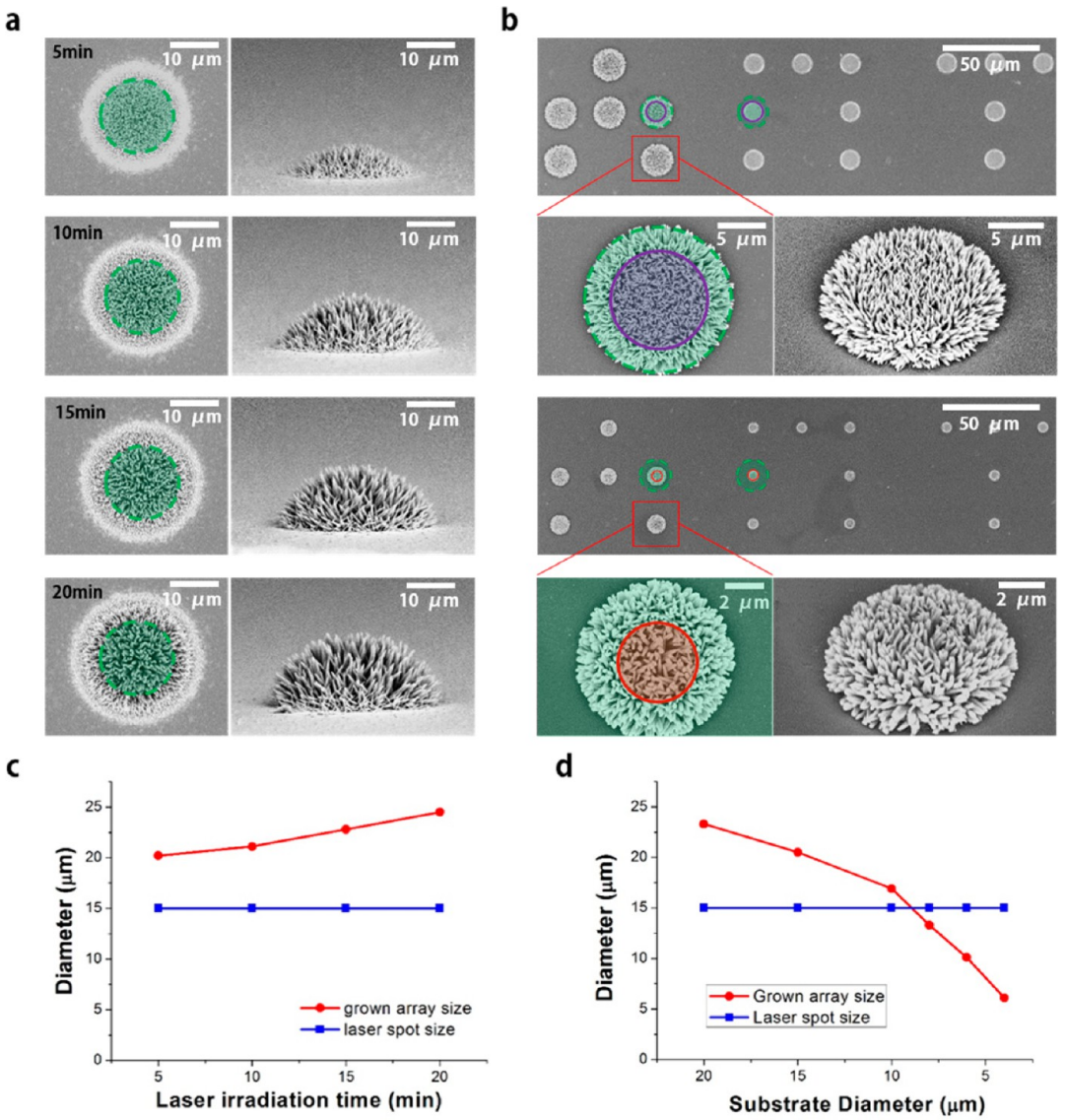

Figure 2. ZnO NW array grown on (a) planar thin Au/Ti layers at different growth time and (b) on the patterned Au/Ti layers with various pattern size (diameters of green, purple and red circles are 15, 10, and 4 μm, respectively). For the planar thin Au/Ti layer, the size of ZnO NW array is always bigger than the laser spot size. On the contrary, the size of ZnO NW array can be comparable or even smaller than the spot size in the case of the array grown on the patterned layer with the same material properties. The diameter of the resultant ZnO NW array grown on planar and patterned Au/Ti layers are plotted according to the irradiation (growth) time and the substrate diameter in (c) and (d).

as polymer films. In this regard, a thin metal layer, which has been implemented as an absorbing layer for a typical LIHG process, is substituted with polyimide (PI) substrate to confirm this idea. Other polymer substrates such as PET and PEN also show very low thermal conductivity as well, however, they are not compatible as a laser absorbing layer for LIHG process because of the high transparency in the visible wavelength. Among various polymer substrates, PI substrate absorbs visible light and was therefore selected as an absorbing layer to provide both low thermal conductivity value (Bulk Au: ~318 W/m·K, PI: 0.1−1 W/m·K)[28−30] as well as an effective photothermal reaction at the surface.

The ZnO NW arrays grown by LIHG process on the PI substrate (commercial UPilex PI film with 250 μm thickness) are shown in Figure 3c−e. The diameter of the resultant ZnO NW is ~15 μm as it can be confirmed from Figure 3e, and it is as small as the one grown on a very thin (30 nm) Au film. This result, plotted on Figure 3b for comparison, confirms that low thermal conductivity efficiently confines the laser-induced temperature field. Being a flexible substrate, PI is vulnerable to high temperature and the substrate can be damaged by a focused laser beam as shown in the ablation line created in Figure 3c and 3d (indicated with the white arrow) at 180 mW laser power. Through careful control of laser power at 60 mW, ZnO NW arrays have been successfully synthesized within the thermal damage. In order to show flexibility of PI substrate unlike rigid substrate,

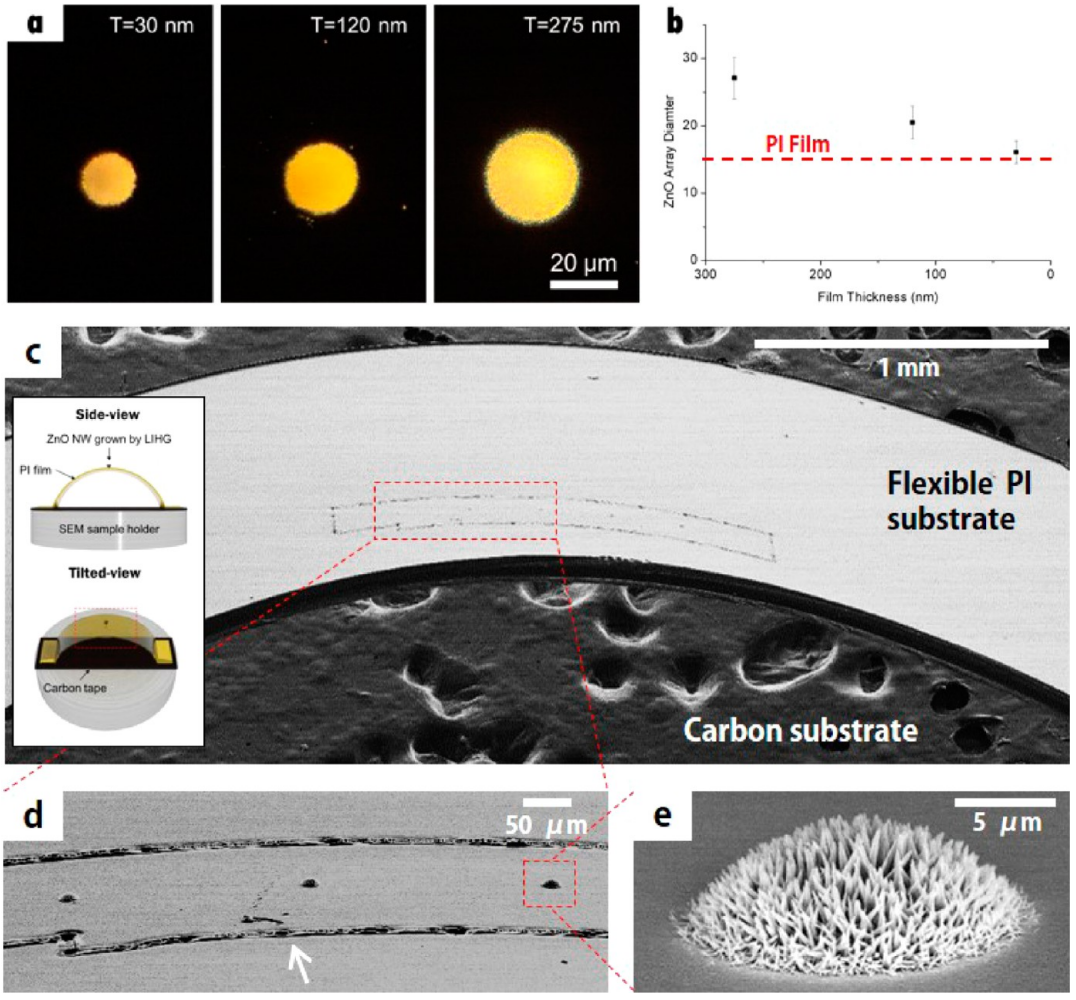

Figure 3. (a) ZnO NW array grown on Au film with various film thicknesses. (b) Thickness dependent ZnO NW array diameter. (c) SEM picture of ZnO NW array grown on a flexible PI substrate. (Inset is a schematics for SEM measurement). (d) Magnified SEM picture of grown ZnO NW array in the red box in panel (c). White arrow indicates the damaged PI obtained at high laser power. (e) Magnified SEM picture of grown ZnO NW array in the red box in panel (d).

SEM image is taken under bending condition of PI substrate in Figure 3c. Also, carbon substrate is placed below PI substrate to prevent charging problem when SEM images are taken as shown in the inset image.

Through elaborate study on the target substrate, we clarify that LIHG process is applicable to other hydrothermally grown NWs as well besides ZnO. Hydrothermal growth of metal-oxide NW except ZnO NW frequently requires a number of harsh environments such as high temperature and severe acidity. As a result, chemically stable substrate such as glass or ceramic is widely used as a template, while an autoclave is a necessity in order to raise the temperature to a sufficient level. While on the other hand, we found that these NWs can be synthesized with LIHG process without any additional equipment such as autoclave.

Our study has been concentrated on seedless growth of TiO_2 NW, which requires 24 h of growth at 120−180 °C in an autoclave within precursor solution at low pH of 1−2 for a conventional bulk growth.[31] By employing the precursor solution used for the conventional growth of TiO_2 NW and following the same LIHG procedure, TiO_2 NW array is grown on the flexible PI substrate as shown in Figure 4 by applying a focused laser for 30 min at 90 mW power. It is apparent from the images that densely packed NWs are selectively grown radially at hemispherical sea-urchin shape on the target substrate similar to the ZnO NW array grown by LIHG process. High magnification images in Figure 4d and 4e reveal that the synthesized nanostructure has tetragonal shape with square top facets. More minute examination on a single NW by high resolution transmission electron microscopy (HR-TEM) at Figure 4f confirms that the NWs are single crystalline TiO_2 at rutile phase, which has interplanar spacing of 0.32 nm along the [110] direction and 0.29 nm along the [001] direction.

In conventional seedless hydrothermal growth of TiO_2 NW, FTO glass is highly recommended as a substrate since FTO glass also has tetragonal rutile structure

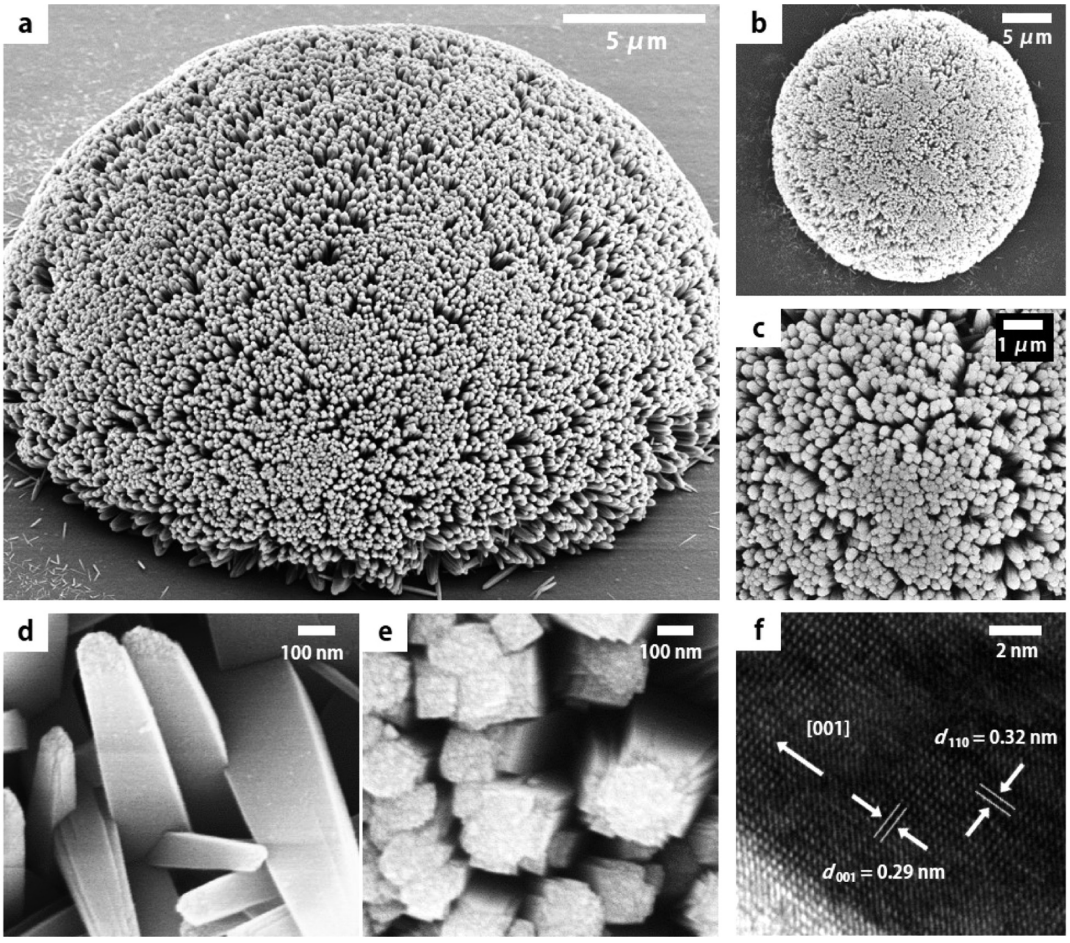

Figure 4. TiO_2 NW array digitally grown on a flexible PI substrate. (a) Tilted SEM image of TiO_2 NW array synthesized by LIHG. (b−e) Magnified SEM images of grown TiO_2 NW. (f) HRTEM image of single TiO_2 NW.

while the lattice mismatch between FTO and rutile TiO_2 is very small to provide a suitable roughness for nucleation and epitaxial growth.[31] Moreover, FTO is chemically stable to the acidic precursor solution which contains hydrochloric acid in order to retard the hydrolysis of titanium butoxide by low pH solution and suppress further growth in side walls by selectively attaching Cl^- ions on the (110) planes of NWs.[32] On the contrary, PI substrate usually has clean surface and does not have property of crystalline structure to satisfy epitaxial growth. In addition, PI substrate is not robust to the acidic solution. Despite these properties, TiO_2 NW can be synthesized on PI substrate by undergoing multiple reactions. Initially, PI substrate immersed in the acidic precursor solution is etched in a small area upon the laser irradiation in a very short time (~15 s). Such unintended etching at the surface provides certain roughness for the nucleation, so that Ti^{4+} precursor hydrolyzes at the etched hole to form crystal nucleus on the PI substrate (~30 s). After the formation of the first TiO_2 crystal nucleus layer, TiO_2 layer is successively deposited on the previously created TiO_2 nanocrystal nucleus layer rapidly (~1 min). Because PI substrate does not have crystalline grain boundary, TiO_2 NW is very densely synthesized on the PI substrate (~5 min) unlike TiO_2 NW grown on a FTO glass with crude grain boundaries. The SEM images at each step as well as the cross-sectional profile of TiO_2 NW array at its complete growth prepared with focused ion beam (FIB) are shown by Figure 5a and Figure 5b.

As above-mentioned, synthesis of TiO_2 NW in a hydrothermal growth usually require considerably high temperature (around 120−180 °C) within a precursor above boiling temperate of water and hydrochloric acid (33%, ~70 °C). It implies TiO_2 NW array can be grown above boiling temperature of precursor under ambient condition by LIHG process. Generally, grown NW array are easily ruined and removed on the substrate when the precursor reaches its boiling point and bubbles are formed. Tiny bubbles at microscale might occur during the growth of TiO_2 NW at its initial stage in particular, yet we could not observe any macroscopic bubbles throughout the entire LIHG process. It is noticeable from Figure 5a that the etching of PI substrate is dominant in the first several seconds. At this stage, we could also notice an increased convective flow, which is different from a common thermal

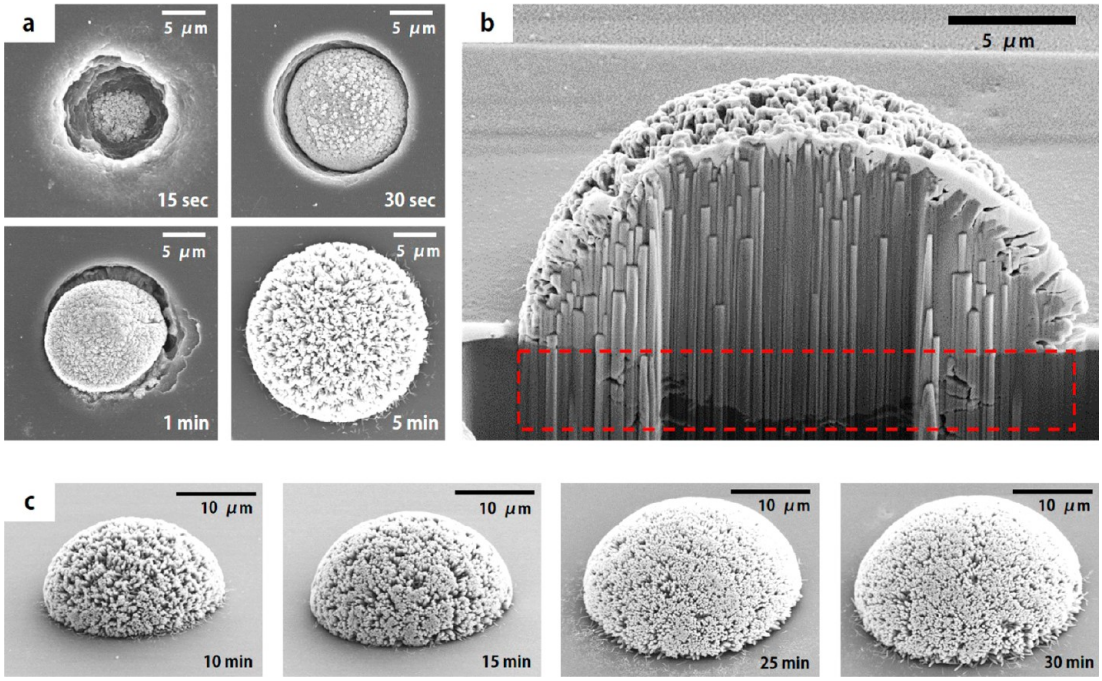

Figure 5. (a) TiO_2 NW growth kinetics on flexible PI substrate at various short laser irradiation time. (b) Cross-sectional image by FIB of grown TiO_2 NW array. (c) TiO_2 NW array growth on a PI substrate with various time at 90 mW.

convection by a point heat source. Such strong convective flow can be explained by the Marangoni flows that are present when bubbles are formed.[33] They, however, do not coalesce and grow into a macroscopic bubble since the surface etching is occurring at the same time. As a result, the effect of bubble is not damaging and TiO_2 NW is successfully synthesized on the PI substrate by LIHG process. Figure 5c shows successful grown TiO_2 NW with various laser irradiation time (from 10 to 30 min) at the laser power of 90 mW.

Assuming that the growth of TiO_2 NW happens at the same conditions as the bulk growth, the growth of TiO_2 NW with LIHG process also offers the possibility of superheating by laser local heating. It has been reported for various types of liquid that the bubble production temperature by laser heating is considerably higher than its macroscopic boiling point (*e.g.*, boiling point: 100 °C, bubble production temperature: 124−146 °C, nucleation temperature: 302.1 °C for H_2O).[34] In this manner, the maximum temperature that is locally induced by the optimum focused laser power may be expected to be higher than the macroscopic bulk boiling temperature of the precursor solution, so that the temperature condition for the synthesis of TiO_2 NW (120−180 °C) is satisfied.

As it has been confirmed that LIHG process is compatible with other hydrothermally grown NWs, multiple NWs can be directly synthesized on the same substrate with consecutive LIHG processes with different precursor liquid. Two different NWs, ZnO and TiO_2, are grown on PI substrate by following the schematics illustrated in Figure 6a. The synthesis of ZnO NW as well as ZnO seeding should be preceded by the growth of TiO_2 NW as ZnO NW can be etched by TiO_2 precursor solution which is largely acidic.

In order to analyze the temperature profile induced by a focused laser about both two NW growth, constant temperature contour (Figure 6b) and temperature profile (Figure 6c) have been calculated by using COMSOL Multiphysics. It is known well that range of proper temperature for ZnO NW growth (60−120 °C) is lower than for range of proper temperature for TiO_2 NW growth (120−180 °C). Therefore, considering initial temperature (T_i) for both NW growth, area of the induced temperature field for ZnO NW growth is larger than that for TiO_2 NW growth under the same experimental condition (same laser power, growth time, and substrate).

Figure 6d shows the SEM images of grown ZnO NW and TiO_2 NW on the same PI substrate by applying LIHG twice with separate precursor solutions. The growth time for each point is fixed to be 5 min, and another experimental conditions are also fixed equally except sort of precursor solution. It has been confirmed that two metal-oxide NW arrays are at different sizes even though same laser power and time are applied on same PI substrate. Through these LIHG processes, we have demonstrated that two heterogeneous NW arrays are facilely synthesized on a flexible substrate at desired positions without using autoclave, while it probably will

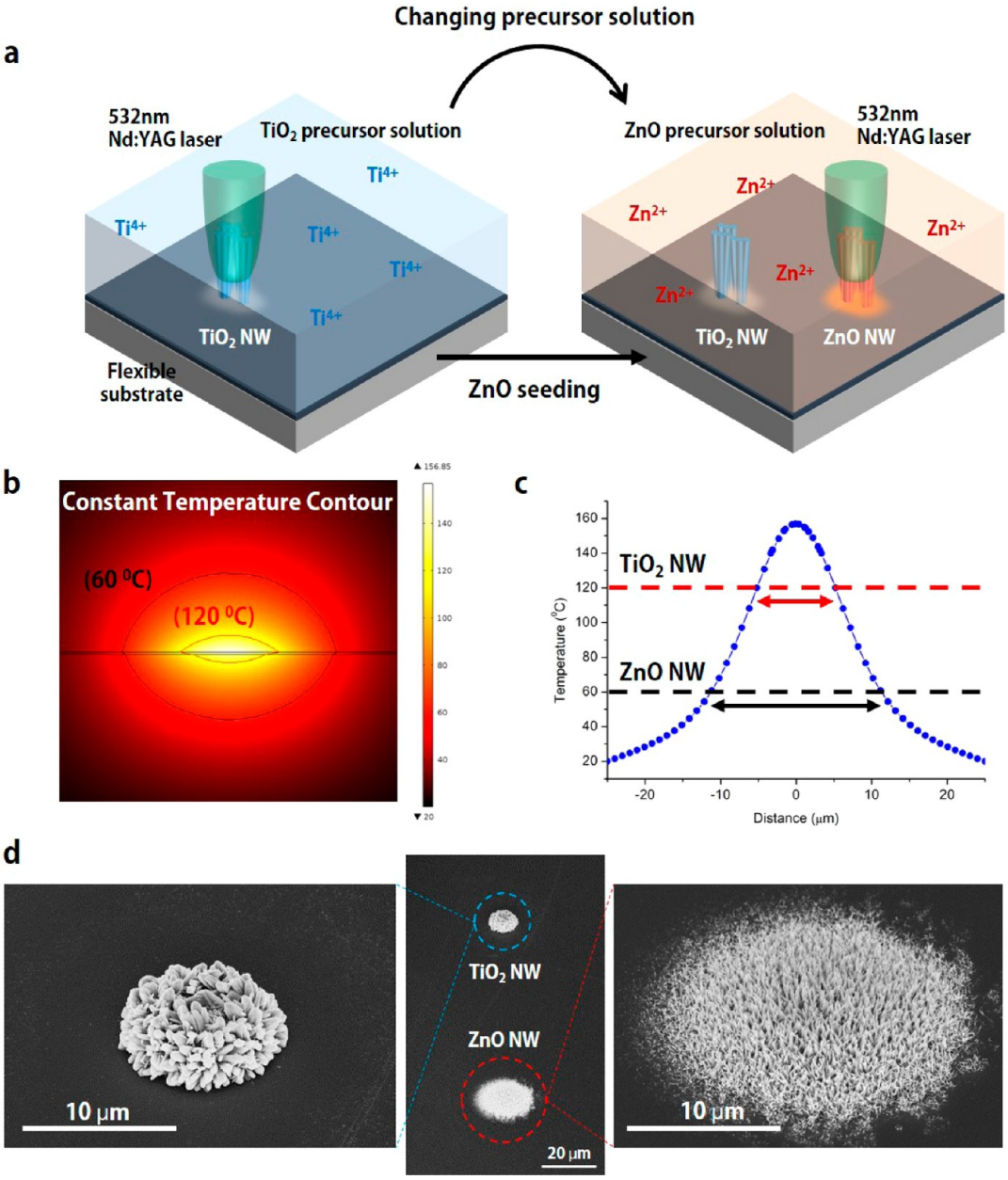

Figure 6. (a) Schematic illustration of the LIHG process for heterogeneous metal-oxide nanowire arrays synthesis on flexible PI substrate. TiO_2 NW array is grown on a flexible substrate immersed in TiO_2 NW precursor solution using a conventional LIHG process. Consequently, the substrate is seeded with ZnO QD, while the surrounding medium is substituted with ZnO precursor solution. By applying other LIHG process, two heterogeneous metal-oxide NW arrays are synthesized on the target substrate. (b) COMSOL simulation on the normalized temperature field profile at the PI substrate. The size of constant temperature contour on 60 °C is larger than that on 120 °C under same laser power applied. (c) Temperature profile at the PI substrate−precursor interface shows the size of induced temperature field for ZnO NW growth is larger than that for TiO_2 NW growth at the same experimental condition. (d) SEM image of TiO_2 NW and ZnO NW grown on the same flexible PI substrate by applying successive LIHG processes. It is noticeable that two metal-oxide NW arrays are at different shapes and sizes even though same laser power and time are applied.

require innumerable steps to achieve similar nanostructure with different techniques.

CONCLUSION

In summary, the influence of the target substrate on LIHG process has been thoroughly investigated in this study. By changing the size and thermal conductivity of the absorbing layer, metal-oxide NW array even smaller than the spot size of the focused laser has been successfully obtained. More importantly, close examination on the target substrate revealed that LIHG process is also compatible to other hydrothermally grown metal-oxide NW as shown in the case of TiO_2 NW grown by LIHG process on PI substrate without autoclave. Through consecutive application of LIHG processes with separate precursor

solutions, heterogeneous metal-oxide NW arrays are easily integrated selectively on a single platform, which is expected to have high potential in multipurpose microsensors.

MATERIALS AND METHODS

ZnO QD Synthesis. 30 mM NaOH in 30 mL of ethanol is added carefully to 10 mM Zinc acetate dehydrate ($Zn(OAc_2)$, Sigma-Aldrich) in 60 mL of ethanol. Then, prepared solution is heated up for 2 h at 60 °C with vigorous stirring and cooled to room temperature. The diameter of synthesized ZnO QD seeds is 5−10 nm with quasi-spherical shape.[35]

ZnO NW Precursor Preparation. For the preparation of ZnO NW precursor, 25 mM of zinc nitrate hexahydrate ($Zn(NO_3)_2 \cdot 6H_2O$, Sigma-Aldrich) and 25 mM hexamethylenetetramine (HMTA, $C_6H_{12}N_4$, Sigma-Aldrich) are mixed in DI water. After then, 5−7 mM polyethylenimine (PEI, C_2H_5N, Sigma-Aldrich) is added and mixture is heated at 95 °C for 1 h and cooled to room temperature. The resulting white precipitates as byproduct are filtered out.[36−38]

TiO_2 NW Precursor Preparation. For the preparation of TiO_2 NW precursor, 30 mL of hydrochloric acid (33% by weight, Sigma-Aldrich) is mixed with 30 mL of DI water with vigorous stirring for 5 min at ambient condition. After then, 1 mL of titanium butoxide is added to the mixture with additional vigorous stirring for 5 min.[31]

LIHG Process. The optical setup of laser-induced hydrothermal growth can be found in the reference paper.[18] The laser beam is focused on the sample through optimally assembled optical setup for LIHG process. In order to generate temperature field on the absorbing layer, 532 nm continuous wave (CW) Nd:YAG laser is used as the optical source. Moreover, commercial objective lens (5X) is used to focus laser spot. For the *in situ* monitoring of growth process, two CCD vision system are placed in the optical setup. More detailed optical setup can be found in the Supporting Information (Figure S7).

Prepared ZnO QDs seeds are uniformly and densely deposited on the various substrates, and the sample is immersed into the prepared ZnO/TiO_2 precursor solution. As sufficient amount of heat has been applied to the absorbing layer during the laser irradiation, ZnO NWs array is synthesized on the substrate within laser-induced temperature field. Similar process is applied for the seedless growth of TiO_2 NW.

Conflict of Interest: The authors declare no competing financial interest.

Acknowledgment. This work is supported by National Research Foundation of Korea (NRF) (Grant No. 2012-0008779), Global Frontier R&D Program on Center for Multiscale Energy System (Grant No. 2012-054172) funded by the Ministry of Science, ICT & Future, and the R&D Convergence Program and ISTK (Korea Research Council for Industrial Science and Technology) (Grant No. B551179-10-01-00), and by Seoul National University, Institute of Advanced Machinery and Design (SNU-IAMD).

Supporting Information Available: Numerical simulation, high resolution SEM, TEM images, process, and experimental setup. The Supporting Information is available free of charge on the ACS Publications website at DOI: 10.1021/acsnano.5b01125.

REFERENCES AND NOTES

1. Kim, F.; Kwan, S.; Akana, J.; Yang, P. Langmuir−Blodgett Nanorod Assembly. *J. Am. Chem. Soc.* **2001**, *123*, 4360–4361.
2. Smith, P. A.; Nordquist, C. D.; Jackson, T. N.; Mayer, T. S.; Martin, B. R.; Mbindyo, J.; Mallouk, T. E. Electric-Field Assisted Assembly and Alignment of Metallic Nanowires. *Appl. Phys. Lett.* **2000**, *77*, 1399–1401.
3. Wang, X.; Summers, C. J.; Wang, Z. L. Large-Scale Hexagonal-Patterned Growth of Aligned ZnO Nanorods for Nano-Optoelectronics and Nanosensor Arrays. *Nano Lett.* **2004**, *4*, 423–426.
4. Pauzauskie, P. J.; Radenovic, A.; Trepagnier, E.; Shroff, H.; Yang, P.; Liphardt, J. Optical Trapping and Integration of Semiconductor Nanowire Assemblies in Water. *Nat. Mater.* **2006**, *5*, 97–101.
5. Hong, S.; Yeo, J.; Manorotkul, W.; Kang, H. W.; Lee, J.; Han, S.; Rho, Y.; Suh, Y. D.; Sung, H. J.; Ko, S. H. Digital Selective Growth of a ZnO Nanowire Array by Large Scale Laser Decomposition of Zinc Acetate. *Nanoscale* **2013**, *5*, 3698–3703.
6. Kwon, J.; Hong, S.; Lee, H.; Yeo, J.; Lee, S.; Ko, S. Direct Selective Growth of ZnO Nanowire Arrays from Inkjet-Printed Zinc Acetate Precursor on a Heated Substrate. *Nanoscale Res. Lett.* **2013**, *8*, 1–6.
7. Ko, S. H.; Lee, D.; Hotz, N.; Yeo, J.; Hong, S.; Nam, K. H.; Grigoropoulos, C. P. Digital Selective Growth of ZnO Nanowire Arrays from Inkjet-Printed Nanoparticle Seeds on a Flexible Substrate. *Langmuir* **2012**, *28*, 4787–4792.
8. Kang, H. W.; Yeo, J.; Hwang, J. O.; Hong, S.; Lee, P.; Han, S. Y.; Lee, J. H.; Rho, Y. S.; Kim, S. O.; Ko, S. H.; Sung, H. J. Simple ZnO Nanowires Patterned Growth by Microcontact Printing for High Performance Field Emission Device. *J. Phys. Chem. C* **2011**, *115*, 11435–11441.
9. Wu, Y.; Yan, H.; Huang, M.; Messer, B.; Song, J. H.; Yang, P. Inorganic Semiconductor Nanowires: Rational Growth, Assembly, and Novel Properties. *Chem.—Eur. J.* **2002**, *8*, 1260–1268.
10. Huber, D. L.; Manginell, R. P.; Samara, M. A.; Kim, B.-I.; Bunker, B. C. Programmed Adsorption and Release of Proteins in a Microfluidic Device. *Science* **2003**, *301*, 352–354.
11. Yang, D.; Kim, D. H.; Ko, S. H.; Pisano, A. P.; Li, Z.; Park, I. Focused Energy Field Method for the Localized Synthesis and Direct Integration of 1D Nanomaterials on Microelectronic Devices. *Adv. Mater.* **2015**, *27*, 1207–1215.
12. Hong, Y. J.; Kim, Y.-J.; Jeon, J.-M.; Kim, M.; Choi, J. H.; Baik, C. W.; Kim, S. I.; Park, S. S.; Kim, J. M.; Yi, G.-C. Selective Formation of GaN-Based Nanorod Heterostructures on Soda-Lime Glass Substrates by a Local Heating Method. *Nanotechnology* **2011**, *22*, 205602.
13. Privorotskaya, N.; Liu, Y.-S.; Lee, J.; Zeng, H.; Carlisle, J. A.; Radadia, A.; Millet, L.; Bashir, R.; King, W. P. Rapid Thermal Lysis of Cells Using Silicon-Diamond Microcantilever Heaters. *Lab Chip* **2010**, *10*, 1135–1141.
14. Kim, J.; Hong, J. W.; Kim, D. P.; Shin, J. H.; Park, I. Nanowire-Integrated Microfluidic Devices for Facile and Reagent-Free Mechanical Cell Lysis. *Lab Chip* **2012**, *12*, 2914–2921.
15. Puigcorbe, J.; Vogel, D.; Michel, B.; Vila, A.; Gracia, I.; Cane, C.; Morante, J. R. Thermal and Mechanical Analysis of Micromachined Gas Sensors. *J. Micromech. Microeng.* **2003**, *13*, 548.
16. Jin, C. Y.; Li, Z.; Williams, R. S.; Lee, K. C.; Park, I. Localized Temperature and Chemical Reaction Control in Nanoscale Space by Nanowire Array. *Nano Lett.* **2011**, *11*, 4818–4825.
17. Yeo, J.; Kim, G.; Hong, S.; Lee, J.; Kwon, J.; Lee, H.; Park, H.; Manoroktul, W.; Lee, M.-T.; Lee, B. J.; *et al.* Single Nanowire Resistive Nano-heater for Highly Localized Thermo-Chemical Reactions: Localized Hierarchical Heterojunction Nanowire Growth. *Small* **2014**, *10*, 5015–5022.
18. Yeo, J.; Hong, S.; Wanit, M.; Kang, H. W.; Lee, D.; Grigoropoulos, C. P.; Sung, H. J.; Ko, S. H. Rapid, One-step, Digital Selective Growth of ZnO Nanowires on 3D Structures Using Laser Induced Hydrothermal Growth. *Adv. Funct. Mater.* **2013**, *23*, 3316–3323.
19. In, J. B.; Kwon, H.-J.; Lee, D.; Ko, S. H.; Grigoropoulos, C. P. *In Situ* Monitoring of Laser-Assisted Hydrothermal Growth of ZnO Nanowires: Thermally Deactivating Growth Kinetics. *Small* **2014**, *10*, 741–749.
20. Yeo, J.; Hong, S.; Manorotkul, W.; Suh, Y. D.; Lee, J.; Kwon, J.; Ko, S. H. Digital 3D Local Growth of Iron Oxide Micro- and

Nanorods by Laser-Induced Photothermal Chemical Liquid Growth. *J. Phys. Chem. C* **2014**, *118*, 15448–15454.
21. Kwon, K.; Shim, J.; Lee, J. O.; Choi, K.; Yu, K. Localized Laser-Based Photohydrothermal Synthesis of Functionalized Metal-Oxides. *Adv. Funct. Mater.* **2015**, *25*, 2222–2229.
22. Hong, S.; Yeo, J.; Manorotkul, W.; Kim, G.; Kwon, J.; An, K.; Ko, S. H. Low-Temperature Rapid Fabrication of ZnO Nanowire UV Sensor Array by Laser-Induced Local Hydrothermal Growth. *J. Nanomater.* **2013**, *2013*, 246328.
23. Ko, S. H.; Pan, H.; Grigoropoulos, C. P.; Luscombe, C. K.; Frechet, J. M. J.; Poulikakos, D. All-Inkjet-Printed Flexible Electronics Fabrication on a Polymer Substrate by Low-Temperature High-Resolution Selective Laser Sintering of Metal Manoparticles. *Nanotechnology* **2007**, *18*, 345202.
24. Paeng, D.; Lee, D.; Yeo, J.; Yoo, J.-H.; Allen, F. I.; Kim, E.; So, H.; Park, H. K.; Minor, A. M.; Grigoropoulos, C. P. Laser-Induced Reductive Sintering of Nickel Oxide Nanoparticles under Ambient Conditions. *J. Phys. Chem. C* **2015**, *119*, 6363–6372.
25. Paeng, D.; Lee, D.; Grigoropoulos, C. P. Characteristic Time Scales of Coalescence of Silver Nanocomposite and Nanoparticle Films Induced by Continuous Wave Laser Irradiation. *Appl. Phys. Lett.* **2014**, *105*, 073110.
26. Son, Y.; Yeo, J.; Moon, H.; Lim, T. W.; Hong, S.; Nam, K. H.; Yoo, S.; Grigoropoulos, C. P.; Yang, D.-Y.; Ko, S. H. Nanoscale Electronics: Digital Fabrication by Direct Femtosecond Laser Processing of Metal Nanoparticles. *Adv. Mater.* **2011**, *23*, 3716–3181.
27. Langer, G.; Hartmann, J.; Reichling, M. Thermal Conductivity of Thin Metallic Films Measured by Photothermal Profile Analysis. *Rev. Sci. Instrum.* **1997**, *68*, 1510–1513.
28. Kurabayashi, K.; Asheghi, M.; Touzelbaev, M.; Goodson, K. E. Measurement of the Thermal Conductivity Anisotropy in Polyimide Films. *J. Microelectromech. Syst.* **1999**, *8*, 180–191.
29. Chen, G.; Hui, P. Thermal Conductivities of Evaporated Gold Films on Silicon and Glass. *Appl. Phys. Lett.* **1999**, *74*, 2942–2944.
30. Bui, C. T.; Xie, R.; Zheng, M.; Zhang, Q.; Sow, C. H.; Li, B.; Thong, J. T. L. Diameter-Dependent Thermal Transport in Individual ZnO Nanowires and its Correlation with Surface Coating and Defects. *Small* **2012**, *8*, 738–745.
31. Liu, B.; Aydil, E. S. Growth of Oriented Single-Crystalline Rutile TiO_2 Nanorods on Transparent Conducting Substrates for Dye-Sensitized Solar Cells. *J. Am. Chem. Soc.* **2009**, *131*, 3985–3990.
32. Feng, X.; Shankar, K.; Varghese, O. K.; Paulose, M.; Latempa, T. J.; Grimes, C. A. Vertically Aligned Single Crystal TiO_2 Nanowire Arrays Grown Directly on Transparent Conducting Oxide Coated Glass: Synthesis Details and Applications. *Nano Lett.* **2008**, *8*, 3781–3786.
33. Iida, Y.; Okuyama, K.; Sakurai, K. Boiling Nucleation on a Very Small Film Heater Subjected to Extremely Rapid Heating. *Int. J. Heat Mass Transfer* **1994**, *37*, 2771–2780.
34. Berry, D. W.; Heckenberg, N. R.; Rubinszteindunlop, H. Effects Associated With Bubble Fformation in Optical Trapping. *J. Mod. Opt.* **2000**, *47*, 1575–1585.
35. Pacholski, C.; Kornowski, A.; Weller, H. Self-Assembly of ZnO: From Nanodots to Nanorods. *Angew. Chem., Int. Ed.* **2002**, *41*, 1188–1191.
36. Greene, L. E.; Law, M.; Goldberger, J.; Kim, F.; Johnson, J. C.; Zhang, Y.; Saykally, R. J.; Yang, P. Low-Temperature Wafer-Scale Production of ZnO Nanowire Arrays. *Angew. Chem., Int. Ed.* **2003**, *42*, 3031–3034.
37. Ko, S. H.; Lee, D.; Kang, H. W.; Nam, K. H.; Yeo, J. Y.; Hong, S. J.; Grigoropoulos, C. P.; Sung, H. J. Nanoforest of Hydrothermally Grown Hierarchical ZnO Nanowires for a High Efficiency Dye-Sensitized Solar Cell. *Nano Lett.* **2011**, *11*, 666–671.
38. Herman, I.; Yeo, J.; Hong, S.; Lee, D.; Nam, K. H.; Choi, J. H.; Hong, W. H.; Lee, D.; Grigoropoulos, C. P.; Ko, S. H. Hierarchical Weeping Willow Nano-Tree Growth and Effect of Branching on Dye-Sensitized Solar Cell Efficiency. *Nanotechnology* **2012**, *23*, 194005.